Restricted Isometry Property in Wave Buoy Analogy and Application to Multispectral Fusion

Taiyu Zhang and Zhengru Ren[®]

Abstract—Real-time sea state information plays a pivotal role in guiding decisions-making for various marine operations. Utilizing the wave buoy analogy (WBA) enables a cost-effective approach to estimating the wave spectrum through ship motion responses, providing an almost real-time estimation of the sea state. However, non-uniformly distributed response amplitude operators (RAOs) bring about performance deterioration in specific sea states, potentially leading to erroneous estimations that could misguide decision-making and result in severe consequences. Nevertheless, it is possible to combine multiple estimates in a rational manner to improve the robustness and accuracy of the WBA. In this study, the restricted isometry property is introduced to evaluate WBA performance. An RAO-driven assessment criterion is proposed to ascertain the reliability of estimates based solely on RAO input. Building upon this assessment criterion, we propose a multispectral fusion algorithm to amalgamate multiple estimates obtained from ships with different geometries and headings, ultimately generating a comprehensive fused result. Numerical experiments are described to demonstrate the proposed algorithm's effectiveness.

Index Terms—Sea state estimation, wave buoy analogy, restricted isometry property, multispectral fusion.

I. INTRODUCTION

NVIRONMENTAL conditions play a crucial role in ensuring the safety and reliability of marine operations. Therefore, in situ sea state information is essential for making informed decisions and providing onboard operational guidance [1], including in activities such as installation and maintenance of offshore structures [2], [3], ship-borne aircraft take-off and landing, ocean shipping [4], [5], etc.

Among the various forms of external loads, waves have the most dominant effect on the hydrodynamic responses of floating structures [6]. Although long-term statistics and weather forecasts can provide an approximate range of significant wave heights and peak wave periods at an operation site, these parameters may not be sufficiently accurate for real-time decision-making. The directional wave spectrum describing the wave energy across different frequencies and directions provides valuable information about the characteristics of

Received 8 January 2024; revised 17 September 2024; accepted 2 November 2024. Date of publication 8 January 2025; date of current version 4 February 2025. This work was supported in part by Shenzhen Science and Technology Program, China, under Grant KJZD20231023100459001; and in part by the Natural Science Foundation of Guangdong Province, China, under Grant 2024A1515011731. The Associate Editor for this article was Y. Zhang. (Corresponding author: Zhengru Ren.)

The authors are with the Institute for Ocean Engineering, Shenzhen International Graduate School, Tsinghua University, Tsinghua Campus, University Town, Shenzhen 518055, China (e-mail: zhengru.ren@sz.tsinghua.edu.cn). Digital Object Identifier 10.1109/TITS.2024.3519199

waves. It can be measured suing several approaches. Meteorological satellite systems can offer an overview of wave statistics across a large sea area, but considering the limitations of low resolution and time delay, they are unsuitable for real-time estimations [7]. Wave radar is another measurement approach [8]. Due to the high cost and need for frequent calibration, however, it is only equipped on a limited number of vessels [9]. Wave rider buoys, compact and robust accelerometer assemblies with pitch and roll sensors, have emerged as a mature solution for sea state estimation [10]. However, these systems are limited to long-term service in fixed sea areas and are not suitable for real-time, in-situ applications. Consequently, there is a shortage of real-time wave information to support marine activities.

Given that a vessel's responses are predominantly driven by sea waves and most vessels are equipped with motion sensors, oscillating ships can be considered as large wave buoys that provide real-time sea state estimates at no additional cost. Consequently, an indirect estimation approach called the wave buoy analogy (WBA) has been proposed [11]. Its theoretical foundation is the near linear relation between the cross-spectra of ship motion and the wave spectrum in the frequency domain. A response amplitude operator (RAO) is the transfer function that relates the vessel's motion to the wave elevation [12]. Depending on the needs for transfer functions, the WBA can be classified as either a model-based or data-driven approach. Model-based methods determine the sea state using a known wave-response model, whereas data-driven methods derive the wave spectrum through online or offline training model.

RAOs are assumed to be perfectly known in the model-based WBA, and both parametric and nonparametric approaches can be employed [13], [14]. In parametric methods, the wave spectrum shape is controlled by several predefined parameters, such as JONSWAP and Bretschneider [15]. The optimal wave parameters are estimated through a nonlinear and nonconvex optimization process that may introduce computational instability [16]. Without any assumptions about the wave spectrum shape, the nonparametric approach is more accurate and flexible [17]. It is better suited to perturbations in the data and allows for a more robust estimation. In nonparametric approaches, the linear system between the response spectra and wave spectrum is discretized into a series of underdetermined equations. The estimation of the sea state is transformed into solving the linear ill-posed problem [18]. Various methods have been employed in earlier works on this topic. The most common technique for addressing inverse problem is convex

optimization [19]. Sparse regression can be introduced to improve the estimation performance under disturbed cross motion spectra. The sparsity and smoothness control terms of the wave spectrum are described in [20]. The Bayesian method provides progressively improved estimates of the wave spectrum through iterative updates of prior probability distributions [21], [22]. To improve computational efficiency, the adaptive Kalman filter was introduced to incorporate future time step measurements as inputs for the current state-space equation, enabling a recursive method [23].

Data-driven methods are gradually gaining popularity as a means of reducing reliance on ship RAOs. A multi-layer classifier is proposed to evaluate the current sea states by extracting features from ship motion data [24]. Additionally, SeaStateNet, a deep neural network designed for sea state classification using the responses of a dynamic positioning (DP) vessel eliminates the need for hand-engineered features [25]. In another approach, a convolutional neural network can be employed to estimate the sea state parameters using ship motion and structural response data collected from container ships [26]. State-of-art artificial intelligence frameworks are also introduced to provide enhanced estimates, free from the hydrodynamic model [27], [28]. While data-driven methods liberate the estimation process from RAO dependency, they still face limitations due to the need for training data. Moreover, computational costs and hardware requirements must also be considered.

The data-based approaches face inherent poor adaptability, making it impractical to train a model for every ship that needs to employ WBA techniques. To address the issue, an uncertainty-aware hybrid approach [16] is proposed, which utilizes both model-based methods and machine learning methods to estimate sea states when training data is limited [29]. The study's conclusions emphasize the importance of model-based estimation, which ensures that WBA can produce reasonably accurate estimates. Consequently, it is crucial to further develop robust and accurate model-based methods to fully utilize and understand the available RAOs. The uncertainties in transfer functions is an inherent problem of the model-based WBA. There exist a fusion estimate solution, using multiple ships simultaneously employed as wave buoys. The frequency-wise variation of wave spectrum estimates is assumed to reflect the level of (un)certainty for each individual estimate and is employed as a weighting parameter [30]. Because ships have complex geometrical forms compared to wave buoys, the non-uniformly distributed transfer functions also induce varying levels of performance when ships encounter waves of diverse directions and frequencies. However, the phenomenon has not been explained in existing studies.

Inspired by compressed sensing, which is similar to the algorithms employed in WBA, the current work aims to demonstrate the performance variation from a mathematical perspective. The restricted isometry property (RIP), which ensures the preservation of distances between all possible sparse signals [31], [32], is introduced to evaluate the quality of WBA estimates. A performance assessment criterion for WBA is proposed, incorporating RIP into the analysis of the

transfer matrix to pre-evaluate the WBA performance using only RAOs as input. Considering that marine operations or shipping often involve multiple ships, a multispectral fusion algorithm is introduced to facilitate scenarios where multiple ships are simultaneously employed as measurement buoys. Building on this criterion, the proposed method enables the combination of estimates from multiple ships to achieve a more precise and comprehensive result. The main contributions of this study are as follows:

- The RIP theory is integrated into to the WBA framework, enabling the accomplishment of performance evaluation before calculation.
- An RAO-driven assessment criterion is pioneeringly proposed to quantify the reliability of the WBA estimates.
 For the first time, the relationship between ship hull and estimate accuracy in various sea states is addressed quantitatively.
- Based on the proposed criterion, a multispectral fusion algorithm is offered to fuse multiple estimates obtained from ships with different geometries and headings.

This study is organized as follows. The notations and preliminary information are introduced in Section I-A. In Section II, the problems with sea state estimation based on ship motion are formulated and typical approaches introduced. The RAO-driven assessment criterion and proposed RIP-based fusion estimation algorithm are described in Sections III and IV, respectively. Numerical experiments are then described in Section V to validate the proposed algorithms. Section VI concludes the study.

A. Notations and Preliminaries

Notations: \mathbb{R}^n and \mathbb{C}^n denote the sets of real and complex n-dimensional spaces, respectively. The imaginary unit is indicated by \mathbf{i} , i,e., $\mathbf{i} = \sqrt{-1}$. For a complex number x, \overline{x} is its complex conjugate, $\Re(x)$ and $\Im(x)$ are its real and imaginary parts, respectively. For a given matrix X, X^{\top} is its transpose, X^* is its Hermite transpose, and $||X||_1$, $||X||_2$, $||X||_F$ are its l_1 -norm, l_2 -norm (Euclidean norm), Frobenius-norm, respectively.

Compressed sensing is a signal processing technique that allows for the recovery of a sparse or compressible signal from a number of measurements smaller than what would traditionally be required. It has applications in various fields, including image processing, medical imaging, and data compression. To recover the original sparse signal from measurements, an ill-posed problem must be solved, i.e.,

$$b = Af, \tag{1}$$

where $b \in \mathbb{R}^m$ is the measurement vector, $A \in \mathbb{R}^{m \times n}$ is the measurement matrix, and $f \in \mathbb{R}^n$ is the unknown sparse data vector. Reconstructing f from a known A and b is an underdetermined problem because m < n. The accuracy of reconstruction depends upon the RIP of measurement matrix, formally defined as follows.

Definition 1 (RIP [33]): For all k-sparse vectors q, most entries are zeros, and there are at most k non-zero entries.

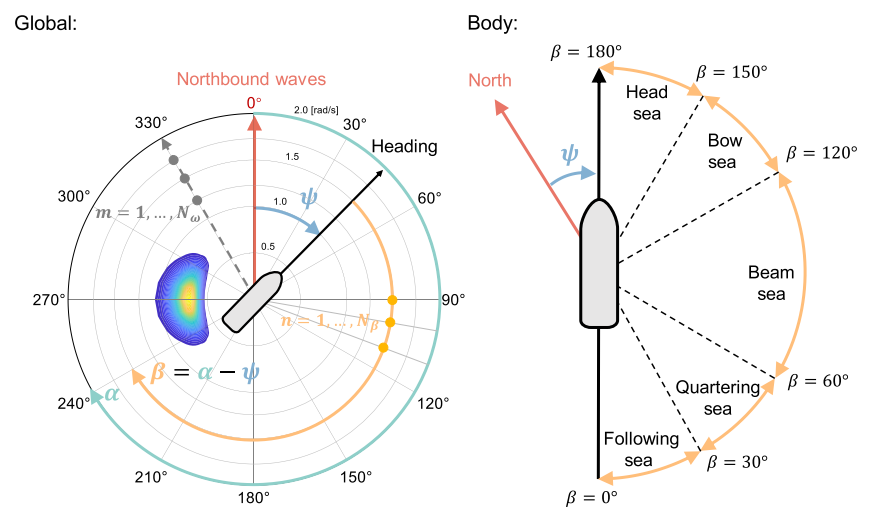


Fig. 1. Discretized wave spectrum in the global and body-fixed reference frame systems.

A measurement matrix A is said to satisfy k-th RIP, which is defined as

$$(1 - \delta)||\mathbf{q}||_2^2 \le ||\mathbf{A}\mathbf{q}||_2^2 \le (1 + \delta)||\mathbf{q}||_2^2, \tag{2}$$

where $0 \le \delta \le 1$. Then, the *k*-th restricted isometry constant (RIC) δ_k is defined as the infimum of all δ , satisfying *k*-th RIP, i.e.,

$$\delta_k := \inf \left\{ \delta : (1 - \delta) ||\boldsymbol{q}||_2^2 \le ||\boldsymbol{A}\boldsymbol{q}||_2^2 \le (1 + \delta) ||\boldsymbol{q}||_2^2, \, \forall \boldsymbol{q} \right\}. \tag{3}$$

Lemma 1 (RIC and eigenvalues [34]): If a measurement matrix **A** satisfies the k-th RIP with RIC δ_k , the following inequality holds,

$$1 - \delta_k \le \lambda_{\min}(A^*A) \le \lambda_{\max}(A^*A) \le 1 + \delta_k, \tag{4}$$

where $\lambda_{\min}(A^*A)$ and $\lambda_{\max}(A^*A)$ denote the minimal and maximal eigenvalues of A^*A , respectively.

II. PROBLEM FORMULATION

A. Coordinate Definition of Discrete Wave Spectrum

The global reference frame has a distribution starting at zero degrees and moves clockwise from true north, while the distribution along a ship's longitudinal axis is referred to as the body-fixed reference frame (see Fig. 1). The WBA regards an oscillating ship as a wave rider buoy to reconstruct the real-time wave spectrum from ship motion responses. Conventionally speaking, the six degrees of freedom (DOFs) motions of a vessel (i.e., surge, sway, heave, roll, pitch, yaw) are indexed by the set $\mathbb{J} = \{1, 2, 3, 4, 5, 6\}$, respectively. The set of DOFs selected in the subsequent calculation is $\mathbb{I} \subseteq \mathbb{J}$. In the present study, for DP vessels, heave, roll, and pitch motions are considered and the influence of the DP system can be neglected [35], i.e., $\mathbb{I} = \{3, 4, 5\}$. The total number of selected DOFs is denoted by N_d .

A directional wave spectrum includes two variables: the frequency ω and incoming wave direction α . In Fig. 1, a wave is moving toward north when $\alpha = 0$. The vessel heading is defined as the longitudinal ship axis with respect to north,

denoted by ψ , and the relative wave heading β represents the incoming wave direction related to the vessel heading, i.e., $\beta = \alpha - \psi$. The wave spectrum distribution to the north is referred to as the global distribution, i.e., $E(\omega, \alpha)$. Conversely, in the body-fixed reference frame, $E(\omega, \beta)$ refers to the distribution along the vessel's longitudinal axis. Depending on the wave heading β , the wave distribution in the body-fixed frame determines the characteristic of the incoming waves. For instance, the beam seas correspond to $\beta \in [\frac{\pi}{3}, \frac{2\pi}{3}] \cup [\frac{4\pi}{3}, \frac{5\pi}{3}]$. The estimation is performed in the body frame and then transformed into the global frame. The vessel heading is measurable and assumed to be known. The directional wave spectrum is discretized into a network with N_{ω} frequencies and N_{β} directions, where N_{ω} is the total number of the wave frequencies and N_{β} is the number of the discrete wave heading directions (see Fig. 1). The indexes of components m and n are defined as $m \in \mathbb{M} = \{1, \dots, N_{\omega}\}$ and $n \in \mathbb{N} = \{1, \dots, N_{\beta}\}$.

B. Wave Buoy Analogy

The cornerstone of the WBA method is the linear relation between ship motions and incoming waves in the frequency domain according to linear wave theory. Assuming that a ship is a linear time-invariant system and the sea state remains steady, linear equations for the response spectra and directional wave spectrum can be constructed in the frequency domain. The RAOs are complex-value transfer functions that can be calculated by hydrodynamic code [36], i.e., $\Phi(\omega, \beta) = \Re(\Phi(\omega, \beta)) + i\Im(\Phi(\omega, \beta))$. The response cross-spectra of a vessel at a specific frequency ω_m is the integral over the wave heading β , expressed as

$$S_{ij}(\omega_m) = \int_{-\pi}^{\pi} \Phi_i(\omega_m, \beta) \overline{\Phi_j(\omega_m, \beta)} E(\omega_m, \beta) \, \mathrm{d}\beta$$

$$\approx \Delta\beta \sum_{n=1}^{N_\beta} \Phi_i(\omega_m, \beta_n) \overline{\Phi_j(\omega_m, \beta_n)} E(\omega_m, \beta_n), \quad (5)$$

where S_{ij} denotes the cross-spectra between the *i*th and *j*th DOFs, Φ_i and Φ_j are the complex transfer functions of the *i*th and *j*th DOFs, and $\Delta\beta$ is the intervals among the discrete

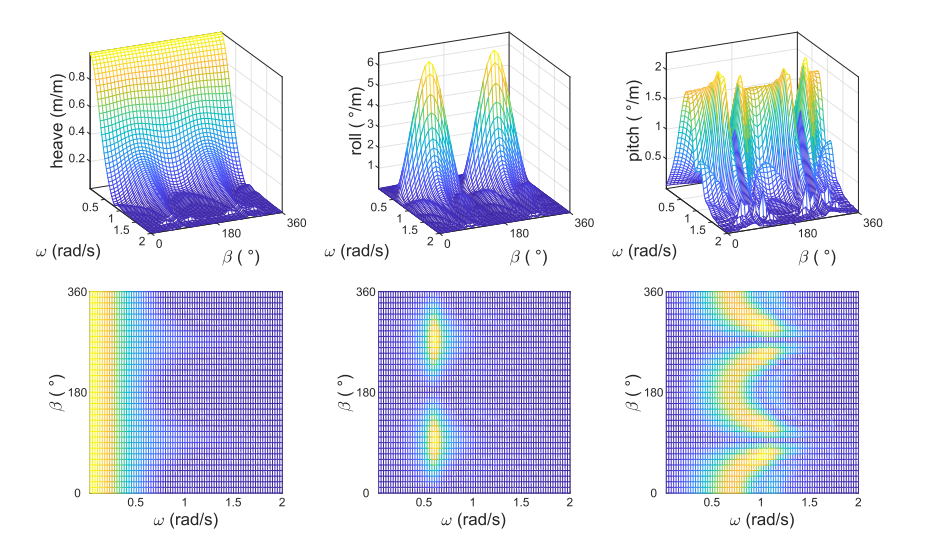


Fig. 2. Motion RAOs of a cargo ship.

 β_n . The cutoff frequency $\omega_{N_{\omega}}$ is selected where the values of the response spectra tend towards zero, i.e., the wave-induced loads excited by the wave components with frequencies larger than $\omega_{N_{\omega}}$ are neglected.

The cross-spectra S_{ij} contains real and imaginary parts. When i=j, $S_{ii}\in\mathbb{R}$; and for $i\neq j$, $S_{ij}\in\mathbb{C}$. Hence, the value of $S_{ij}(\omega_m)$ can be divided into three parts: $S_{ii}(\omega_m)$, $\Re(S_{ij}(\omega_m))$, and $\Im(S_{ij}(\omega_m))$. Equation (5) can also be rewritten as the three-part expression, i.e., $\Phi_i(\omega_m,\beta_n)\overline{\Phi_j(\omega_m,\beta_n)}=\Re(\Phi_i)\Re(\Phi_j)+\Im(\Phi_i)\Im(\Phi_j)+$ i $\left[\Im(\Phi_i)\Re(\Phi_j)-\Re(\Phi_i)\Im(\Phi_j)\right]$. Therefore, for a specific frequency ω_m , there exists a total of N_d^2 equations, which can be rewritten into a vectoral form

$$b_m = A_m f_m, (6)$$

where $b_m \in \mathbb{R}^{N_d^2}$, $A_m \in \mathbb{R}^{N_d^2 \times N_\beta}$, and $f_m \in \mathbb{R}^{N_\beta}$, given as (7), shown at the bottom of the page.

Rewriting the equations for all frequency components into a vector form yields

$$h = Af \tag{8}$$

where $b = [b_1^\top, b_2^\top, \dots, b_{N_\omega}^\top]^\top \in \mathbb{R}^{N_d^2 N_\omega}$, $A \in \mathbb{R}^{N_d^2 N_\omega \times N_\beta N_\omega}$, and $f = [f_1^\top, f_2^\top, \dots, f_{N_\omega}^\top]^\top \in \mathbb{R}^{N_\beta N_\omega}$. The wave spectrum estimation is transformed into the solving of an underdetermined linear equation (8). Solving such an ill-posed problem

encounters numerical issues, including the lack of a unique solution and sensitivity to perturbations [37].

C. Performance Deterioration of the WBA

Ships have different geometric shapes from those of spherical wave buoys. The hydrodynamic response of a given cargo ship under incoming waves is significantly influenced by the wave direction and frequency (see Fig. 2). According to the RAOs, the heave motion exhibits a lowpass characteristic; there is almost no roll motion in head seas or following seas, and very low pitch responses are noticed in beam seas. Non-uniformly distributed RAOs contribute to the performance deterioration of the WBA under specific sea states. A number of simulations were conducted to illustrate the variance.

The predefined sea state is assumed to be the product of a long-crested wave spectrum and spreading function, given by

$$E(\omega, \alpha) = S(\omega)D(\alpha)$$
.

$$S(\omega) = \frac{H_s^2 \left[((4\lambda + 1)/4)\omega_p^4 \right]^{\lambda}}{4\Gamma(\lambda)\omega^{4\lambda + 1}} \exp\left[-\frac{4\lambda + 1}{4} \left(\frac{\omega_p}{\omega} \right)^4 \right],$$

$$D(\alpha) = \frac{2^{2s - 1}\Gamma^2(s + 1)}{\pi\Gamma(2s + 1)} \cos^{2s} \left(\frac{\alpha - \alpha_p}{2} \right), \tag{9}$$

where H_s is the significant wave height, ω_p is the peak angular frequency, α_p is the mean wave direction, Γ is the Gamma

$$b_{m}(\omega_{m}) = \begin{bmatrix} S_{ii}(\omega_{m}), \dots, \Re(S_{ij}(\omega_{m})), \dots, \Im(S_{ij}(\omega_{m})), \dots \end{bmatrix}^{\top},$$

$$A_{m}(\omega_{m}) = \Delta\beta \begin{bmatrix} \dots & \Re(\Phi_{i}(\omega_{m}, \beta))\Re(\Phi_{i}(\omega_{m}, \beta)) + \Im(\Phi_{i}(\omega_{m}, \beta))\Im(\Phi_{i}(\omega_{m}, \beta)) & \dots \\ \vdots & & & \vdots \\ \dots & \Re(\Phi_{i}(\omega_{m}, \beta))\Re(\Phi_{j}(\omega_{m}, \beta)) + \Im(\Phi_{i}(\omega_{m}, \beta))\Im(\Phi_{j}(\omega_{m}, \beta)) & \dots \\ \vdots & & & \vdots \\ \dots & \Im(\Phi_{i}(\omega_{m}, \beta))\Re(\Phi_{j}(\omega_{m}, \beta)) - \Re(\Phi_{i}(\omega_{m}, \beta))\Im(\Phi_{j}(\omega_{m}, \beta)) & \dots \end{bmatrix},$$

$$f_{m}(\omega_{m}) = \begin{bmatrix} E(\omega_{m}, \beta_{1}), E(\omega_{m}, \beta_{2}), \dots, E(\omega_{m}, \beta_{N_{\beta}}) \end{bmatrix}^{\top}.$$

$$(7a)$$

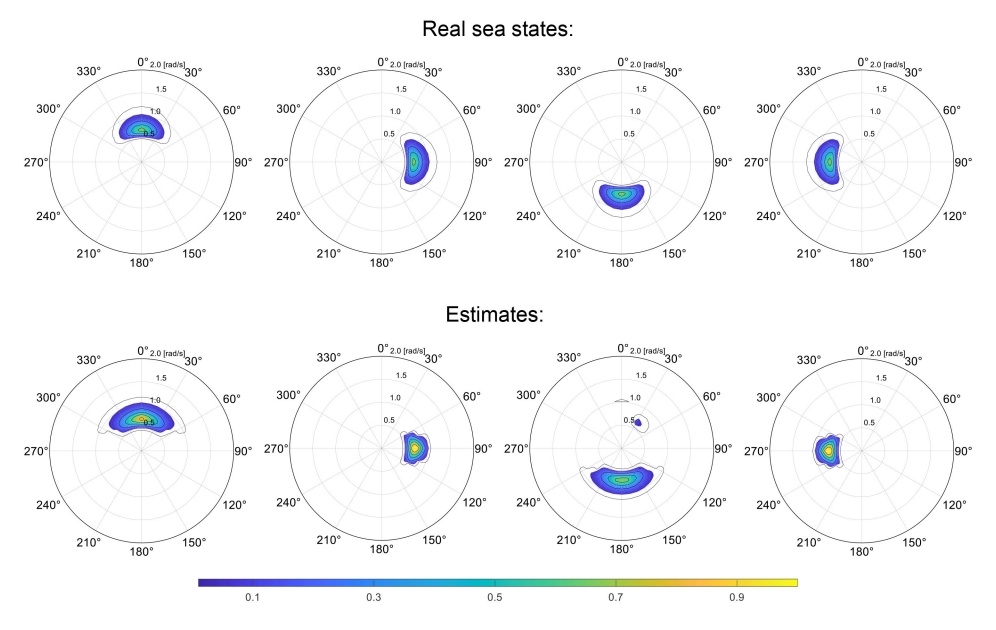


Fig. 3. Predefined sea states in a special range of wave headings and corresponding estimates from the WBA (from left to right, the mean wave headings are 0° , 90° , 180° , and 270°).

function, and s and λ are the shape parameters. Ship responses are simulated under predefined sea states, followed by a crossspectral analysis. It is assumed that the sea states remain stable throughout a 300-second sampling period.

The nonparametric method is applied to reconstruct the real-time wave spectrum. To calculate the vector-form wave spectrum f from the transfer matrix A and response spectra b, additional constraints and prior information are introduced. The wave spectrum estimate \hat{f} is received by solving the following cost function, i.e.,

$$\begin{split} \hat{f} &= \arg\min_{f} \, ||Af - b||_2^2 + \gamma_1 ||f||_2^2 + \gamma_2 ||Df||_1, \qquad (10a) \\ &\text{s.t. } f \geq 0 \,, \end{split} \label{eq:force_force}$$

s.t.
$$f > 0$$
, (10b)

$$f_1 = 0, (10c)$$

$$f_{N_{co}} = 0, (10d)$$

where D matrix can provide second-order differences of estimated wave spectra in terms of frequency and direction, and γ_1 , γ_2 , and γ_3 are tuning parameters that provide trade-offs between accuracy and smoothness. By setting suitable tuning parameters, unsmooth estimates are less likely to be accepted. The real wave spectrum is non-negative and tends to approach zero in both the high and low frequency regions. Hence, additional constrains are considered: (10b), (10c), and (10d). By reshaping the optimal \hat{f} into a matrix denoted as \hat{E} , we obtain the estimate of the directional wave spectrum representing the current sea state.

A series of simulations are included below to illustrate the performance deterioration under different sea states (see Fig. 3 and Fig. 4). The colorbar represents the distribution of wave spectrum energy, with the blue indicating zero energy and yellow representing the upper limit. Fig. 3 presents the WBA estimates in the same sea state with different headings. Poor estimation can be seen in head seas, beam seas, and following seas, and the disparities are significant. The shapes of the estimates in the head and following seas are dispersive, as indicating in the first and third columns of Fig. 3. Furthermore, the energy distribution of the estimated spectra are concentrated and peak energy higher in beam seas, as compared to the real wave spectra shown in the second and forth columns of Fig. 3.

Figure 4 presents the WBA estimate of sea states with a constant H_s and varying T_p . In the frequency domain, the ship acts like a lowpass filter when facing incoming waves, attenuating high-frequency motion responses. Hence, the WBA exhibits only a limited ability for high-frequency waves. As depicted in the first column of Fig. 4, the WBA precisely restores the distribution of wave energy when the peak wave period is 8 s. However, the estimates from the WBA deteriorate with the decreasing peak wave period T_p , resulting in the scattered low-frequency and attenuated high-frequency portions. Furthermore, when the peak wave period reduces to 5 s, the WBA estimation completely fails (see the last column of Fig. 4). The performance degradation encountered with the WBA is inevitable, due to a ship's inherent hydrodynamic characteristics.

D. Problem Statement

The WBA estimate from a specific ship is not consistently reliable, and ships may experience performance deterioration in specific sea states. Erroneous sea state estimations can lead to deviations in decision-making, potentially resulting in severe consequences.

The present study aims to provide a theoretical explanation for the performance variations observed in the WBA. The phenomenon primarily stems from the ship's non-uniformly distributed wave-to-motion response properties. By further investigating and analyzing the inherent response functions, the research attempts to propose an assessment criterion to evaluate the reliability and accuracy of a specific ship's WBA performance. Given that marine operations often involve

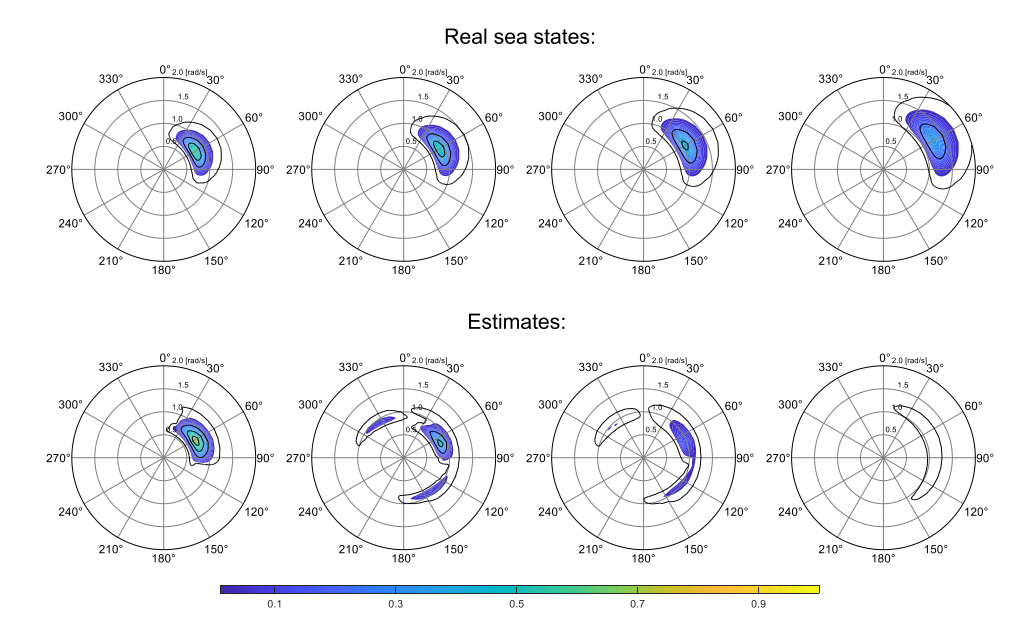


Fig. 4. Progressively less accurate estimates obtained from the WBA as the incoming sea states transition towards higher frequencies (from left to right, the peak wave periods are 8 s, 7 s, 6 s, and 5 s).

multiple vessels with different geometric shapes and operational headings, it is feasible to fuse sea state estimates from different vessels to obtain more accurate and robust measurements. We envision a scenario where multiple ships are simultaneously employed as measurement buoys, using the proposed assessment criterion as the basis for weight distribution, thereby reducing the impact of erroneous results on the estimates and improving overall reliability.

III. ASSESSING THE WBA PERFORMANCE USING RIP

A. Restricted Isometry Property

Compressed sensing is a revolutionary technique in data acquisition and signal recovery. It is a mathematical framework that allows for the efficient acquisition and reconstruction of sparse or compressible signals by resolving an inverse problem. The key factors in compressed sensing are the sparse representation of signals and construction of the measurement matrix. RIP, as defined in (2), is a crucial property for constructing the measurement matrix because it ensures the preservation of the distances between all possible sparse signals. RIC, denoted as δ_k , is a quantitative measure employed to assess how well a matrix satisfies the RIP condition. A small δ_k indicates that the measurement process minimally distorts the distances between sparse vectors, which is essential for achieving accurate signal recovery. The RIC is related to the smallest and largest eigenvalues of the measurement matrix [38].

Estimating the wave spectrum from ship motions exhibits considerable similarity to signal recovery processes. First, they are both solving an ill-posed inverse problem. And the spectral power distribution of waves also shows sparse characteristics because wave energy is concentrated within a narrow range of wave periods and directions. Even a multiple peak spectrum retains the sparsity. Specifically, for a $36 \times$

100 matrix, most elements are zero or close to zero. The sparsity is reason that most regression optimizations often use a LASSO structure to address such problems. Hence, the inverse problem of the WBA can be equivalent to signal recovery, and the transfer matrix in (8) is equivalent to the measurement matrix in (1). Instead of a randomly constructed measurement matrix, the transfer matrix in the WBA depends on the RAOs. Unevenly distributed RAOs lead to disparities in the eigenvalues, subsequently affecting the RIC distribution of the transfer matrix. Variations in the RIC distribution explain the discrepancies in computational accuracy across different sea states. Accordingly, the performance deterioration of the WBA can be analyzed from the RIC perspective.

B. Algorithm for Local RIC Estimation

To explain the performance variations in the WBA, an algorithm is proposed here to calculate the local RIC (summarized in Algorithm 1). To limit the range of the RIC, the transfer matrix constructed by RAOs is normalized into an interval of 0 to 1. The selection of the sparse order k and frequency range r_{ω} is determined in alignment with the narrow bandwidth characteristics found in the power distribution of the wave spectrum. For specific ranges of wave frequency and heading, the block matrix A_{mn} is partitioned from the transfer matrix A. The RIC of the blocked matrix A_{mn} (namely, the local RIC) serves as a measure to evaluate the WBA performance.

Remark 1: To ensure the robustness of the local RIC calculation, a total of h_s random column sampling processes are employed. First, column vectors are extracted from the block matrix \mathcal{A}_{mn} , according to randomly permuted indexes p. The extracted columns are then used to construct an Hermite matrix, denoted by $\mathcal{S}^{\top}\mathcal{S}$. The eigenvalues Λ of the Hermite matrix are obtained through singular value decomposition.

Algorithm 1 Local RIC Calculation

```
Input: RAOs of a specific ship, sparse order k, range of frequency r_{\omega}, sample size h_s
Output: Assessment criterion \Delta, overall performance criterion \Theta
 1: Construct the transfer matrix A with a size of N_d^2 N_\omega \times N_\beta N_\omega from RAOs, and normalize it into 0-1 interval, denote as
           \mathcal{A} = A/\max(\operatorname{abs}(A));
 2: for n \leftarrow 1:N_{\beta} do
                                                                                                                                                  > Traverse in all directions
                                                                                                                                                ▶ Traverse in all frequencies
 3:
           for m \leftarrow r_{\omega} + 1: N_{\omega} - r_{\omega} do
                 \mathcal{A}_{mn} \leftarrow \mathcal{A}[:, nN_{\omega} + m - r_{\omega} : nN_{\omega} + m + r_{\omega}];
                                                                                                                                              ▶ Matrix block decomposition
 4:
                 n_{col} \leftarrow 2r_{\omega} + 1;
 5:
                 for h \leftarrow 1: h_s do
                                                                                                                               \triangleright h_s times of random column sampling
 6:
                      \mathbf{p} \leftarrow \text{randperm}(n_{col}, k);
                                                                                                                                \triangleright Create k random indices within n_{col}
 7:
                      \mathcal{S} \leftarrow \mathcal{A}_{mn}[:, \mathbf{p}];
                                                                                                                                  ⊳ Column sampling from block matrix
 8:
                      \Lambda \leftarrow \text{eigenvalues}(\mathcal{S}^{\top}\mathcal{S});
                                                                                                                                 ▶ Calculate the eigenvalues using SVD
 9:
                      if max(\Lambda) \ge 1 then
10:
                           \delta(h) \leftarrow \max(\max(\Lambda) - 1, 1 - \min(\Lambda));
                                                                                                                                       \triangleright RIC calculation based on Eq.(4)
11:
                      else
12:
                           \delta(h) \leftarrow 1 - \min(\Lambda)
                                                                                                                                       \triangleright RIC calculation based on Eq.(4)
13:
                      end if
14:
15:
                 \hat{\delta}(m,n) \leftarrow \frac{1}{h_s} \sum_{h=1}^{h_s} \delta(h);
                                                                                                                         \triangleright Local RIC value corresponding to \omega_m, \beta_n
16:
17:
18: end for
19: \Delta \leftarrow \hat{\delta}/\max(abs(\hat{\delta})), \Theta \leftarrow ||1 - \Delta||_F
```

TABLE I
GEOMETRIC PARAMETERS OF THE THREE SHIPS

Geometry	Ship1	Ship2	Ship3
Length (m)	52	55	98
Breadth (m)	8	12	15
Draught (m)	3	4	6

Subsequently, the RIC of each block matrix is calculated using (4). The corresponding local RIC $\hat{\delta}(m,n)$ is obtained through the averaging of outcomes from each random column sampling process.

Remark 2: By traversing a variety of wave directions and frequencies, local RICs contribute to the comprehensive evaluation of the WBA performance. To ensure the comparability of criteria across different ships, the local RICs are normalized to fall within the 0 to 1 interval, thereby establishing the assessment criterion referred to as Δ . Furthermore, the overall performance of a specific ship can be quantified by calculating the Frobenius norm of $(1 - \Delta)$, denoted by Θ .

C. Assessment Criterion Based on the Local RIC

In compressed sensing, a measurement matrix with a lower RIC leads to superior signal recovery. Similarly, under a specific sea state with a peak wave frequency of ω_m and mean wave heading of β_n , the WBA exhibits a better performance when the value of the corresponding local RIC $\Delta(m, n)$ is lower. The aforementioned pattern serves as the assessment criterion, which can be derived depending only on the RAOs.

An illustrative example using three ships described below to validate the proposed assessment criterion; the ships' geometric parameters are listed in TABLE I. To establish the assessment criterion Δ of each ship, Algorithm 1 was

employed with a sparse order k = 10 and a frequency range of $r_{\omega} = 5$. The sample size was set at $n_s = 1,000$. For the three ships, their respective local RIC distributions across frequencies and directions are depicted in Fig. 5(a).

A substantial number of simulations was used to provide further validation of the proposed assessment criterion. The simulation process aligned with the methodology proposed in Section II-C. To evaluate the estimation performance, a parametric sweep was conducted by varying the wave directions α_p and peak wave periods T_p within the ranges of 0 to 360° and 3 to 20 s, respectively. It is noteworthy that the ideal response spectra, obtained through the multiplication of the transfer matrix and predefined wave spectra were utilized to prevent disturbances stemming from inaccurate response cross-spectra. The mean square error (MSE) was employed to compare the real wave spectrum with the estimates, given by

$$MSE = \frac{1}{N_{\omega}N_{\beta}}|f - \hat{f}|^2, \tag{11}$$

where f denotes the vector form of the real wave spectrum and \hat{f} is the estimate derived from (10). Fig. 5(b) displays the estimation errors for the three ships across various sea states.

As shown in Fig. 5, the patterns observed in the distributions of estimation errors for the three ships were consistent with the distributions of their respective local RIC values. The simulation results aligned with the proposed assessment criterion, such as suboptimal performance under extremely high and low frequency waves and reduced effectiveness when facing waves at special headings. Additionally, the distributions of RIC values corresponding to the ships' estimation errors showed that lower RIC values corresponded to lower MSE, i.e., more accurate estimates. All three ships, despite their different geometries, exhibited similar patterns. This robustly validated

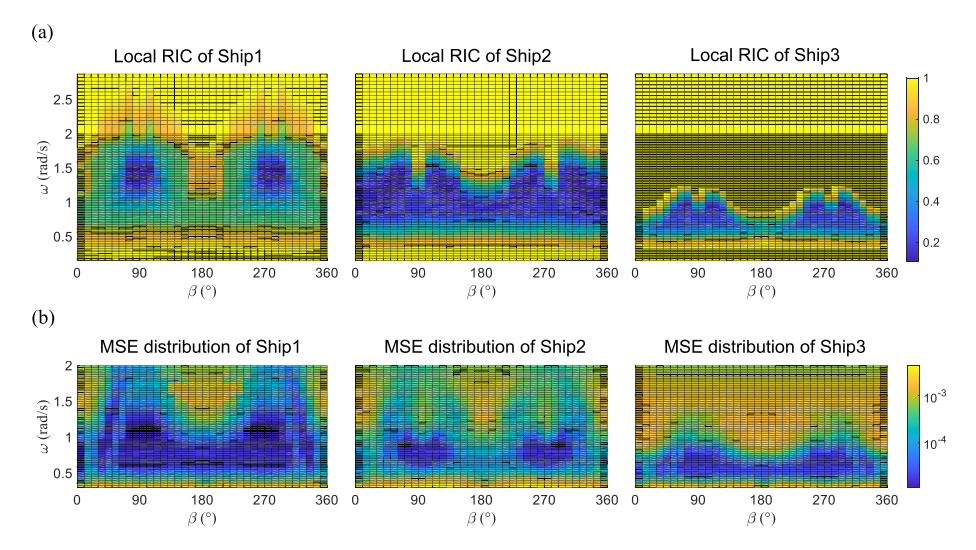


Fig. 5. (a) Local RIC distributions of three ships across various frequencies and directions; (b) Distributions of WBA estimation errors of the three ships when encountering waves from various frequencies and directions.

the effectiveness of the proposed assessment criterion. The results will be further discussed in Section V.

IV. MULTISPECTRAL FUSION

With the support of the proposed RAO-driven assessment criterion, it becomes possible to pre-evaluate the WBA performance using the main wave features (mean wave direction and frequency). Consequently, the criterion can serve as the foundation for scenarios where multiple ships are simultaneously employed. Under a specific sea state, the criterion provides a quantitative measure of the reliability and accuracy of estimates from each ship, serving as the basis for weight distribution. Ships corresponding to lower local RIC values under the current sea state are considered more reliable. By employing this approach, the influence of inaccurate estimates can be restrained or even eliminated, while the contribution of accurate estimates is given more weight. As a result, the fusion results will be more robust. The whole multispectral fusion algorithm is summarized in Fig. 6.

Remark 3: The indexes of multiple ships are defined as $q \in \mathbb{Q} = \{1, \cdots, N_{\text{Ship}}\}$. Using Algorithm 1, the assessment criteria and overall performance of multiple ships can be established beforehand. The priority of the fusion algorithm involves obtaining the peak frequency ω_m and mean wave heading β_n for each estimate. Then, the local RIC $\Delta_q(m,n)$ and overall performance Θ_q both contribute to the weighted parameter μ_q . When μ_q exhibits a high value for a specific ship, the estimate is considered reliable, resulting in a higher weight assignment during the fusion process. Conversely, if μ_q falls below the threshold value η , the estimate is regarded as unreliable and makes no contribution to the fusion process. Whereafter, a frame transformation is executed. Multiple directional wave spectra are fused in the global frame, utilizing the weighted parameter μ_q .

Remark 4: If the maximum value of $\{\mu\}$ fall below the threshold value, the fusion algorithm designates the estimate with the highest weight as the ultimate estimate.

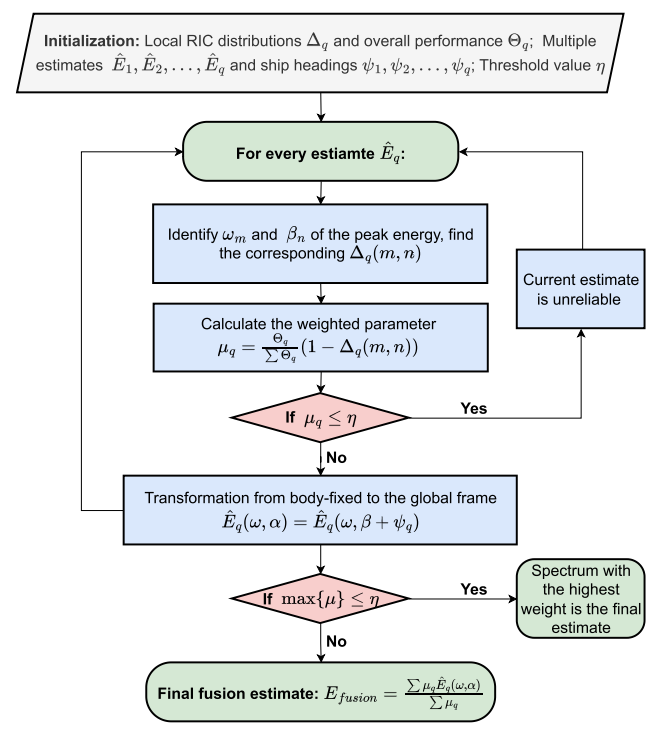


Fig. 6. Flow chart for the multispectral fusion algorithm.

V. SIMULATION

A. Overview

Numerical simulations were implemented to verify the RIP-base fusion algorithm. Three different DP ships with various geometric shapes and hydrodynamic coefficients were employed, as listed in TABLE I. The sea state was assumed to be stationary during a 300-second sampling period. The directional wave spectrum, predefined using (9), was discretized into a 100×36 grid. A angular frequencies from 0.03 to 3.14 rad/s were considered, and $N_{\omega} = 100$. Wave headings from 0° to 360° were discretized into angles with intervals of 10° , so N_{β} equaled 36.

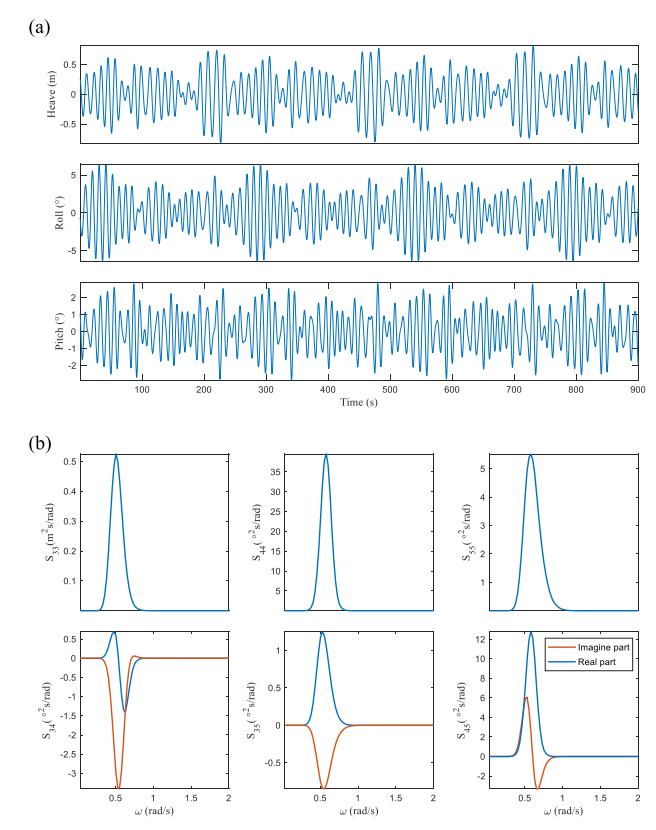


Fig. 7. Time series and motion response spectra.

Regarded as the superposition of waves from different directions and frequencies interacting with the RAOs, ship responses could be expressed as follows

$$r(t) = \sum_{m=1}^{N_{\omega}} \sum_{n=1}^{N_{\beta}} a_{mn} \cos(\omega_m t + \phi_{mn} + \epsilon_{mn}), \qquad (12a)$$

$$a_{mn} = |\Phi(\omega_m, \beta_n)| \sqrt{2E(\omega_m, \beta_n)\Delta\omega\Delta\beta},$$
 (12b)

$$\phi_{mn} = |\Psi(\omega_m, \rho_n)| \sqrt{2E(\omega_m, \rho_n)} \Delta \omega \Delta \rho, \qquad (12b)$$

$$\phi_{mn} = \arctan(\frac{\Im[\Phi(\omega_m, \beta_n)]}{\Re[\Phi(\omega_m, \beta_n)]}), \qquad (12c)$$

where a_{mn} is the motion amplitude at specific frequency ω_m and wave heading β_n , ϕ_{mn} contains the phase information for the RAO, ϵ_{mn} is the random phase angle, and $\Delta\omega$ and $\Delta\beta$ are the increments of the discrete directions and frequencies. By selecting an appropriate window size and overlap length, the Welch method was adopted to calculate the cross-spectra. The time series and corresponding cross-spectra of a specific ship are presented in Fig. 7.

A set of predetermined sea states, as detailed in TABLE II, were employed in simulations to showcase the effectiveness of the multispectral fusion algorithm. The significant wave height H_s , peak period T_p , and shape coefficient s were randomly selected within the ranges of 1 to 1.8 m, 5 to 15 s, and 17 to 23, respectively. The selection of wave height is due to the WBA theory's inability to address nonlinearity under high seas; hence, moderate sea states were considered, where the significant wave height and wave period within the most commonly used range 1-1.8 m and 5-15 s, respectively. The spreading parameters were chosen based on common

TABLE II Environmental Parameters and Ships' Headings

No.	H_s (m)	α_p (°)	T_p (s)	s (-)	ψ_1 (°)	ψ_2 (°)	ψ ₃ (°)
1	1.57	149.4	6.8	23	130	110	90
2	1.33	141.8	8.7	22	170	130	60
3	1.46	12.6	9.2	19	170	70	170
4	1.6	305	6	21	30	150	40
5	1.55	147	12.1	19	70	80	120
6	1.4	11.9	6.9	21	170	10	100
7	1.68	265.5	5.2	20	0	70	150
8	1.22	273.2	6.5	23	40	100	130
9	1.64	78	12.4	20	90	20	100
10	1.29	92.2	8.3	22	170	80	100
11	1.27	97.4	14.9	20	40	90	170
12	1.47	140.8	8.2	21	40	100	40
13	1.24	133.1	6.2	22	90	50	60
14	1.31	283.9	8.5	22	90	60	80
15	1.45	230.6	7.1	17	60	100	80
16	1.3	324.8	7.5	17	60	150	50
17	1.53	121.9	8.6	17	80	140	50
18	1.28	38.9	8.4	22	10	20	80
19	1.62	154.1	6.2	22	80	40	110
20	1.67	262.9	8.3	22	100	160	50

TABLE III WEIGHT DISTRIBUTIONS AND MEAN SQUARE ERRORS OF ESTIMATES

	Weight (-)			Mean square error (m ² s/rad)			
NO.	Ship1	Ship2	Ship3	Ship1	Ship2	Ship3	Fusion
1	0.32	0.39	0.29	1.40E-03	4.90E-04	1.12E-03	3.70E-04
2	0.44	0.56	0	4.26E-04	1.05E-04	4.76E-04	8.73E-05
3	0	1	0	9.07E-04	8.23E-05	8.96E-04	8.23E-05
4	0.49	0.51	0	1.67E-03	1.15E-03	2.27E-03	4.42E-04
5	0	1	0	4.20E-04	4.17E-04	2.93E-03	4.17E-04
6	0	0.59	0.41	5.57E-04	6.65E-04	5.28E-04	3.23E-04
7	0.55	0.45	0	8.03E-04	1.21E-03	2.56E-03	4.96E-04
8	0.44	0.56	0	3.41E-04	3.44E-04	6.73E-04	8.44E-05
9	0	1	0	4.99E-04	3.44E-04	1.57E-03	3.44E-04
10	0.43	0.57	0	4.77E-04	2.75E-04	5.03E-04	1.23E-04
11	1	0	0	4.15E-04	4.73E-04	4.49E-04	4.15E-04
12	0	1	0	8.12E-04	7.57E-05	8.67E-04	7.57E-05
13	0.30	0.43	0.26	4.51E-04	3.91E-04	9.38E-04	1.67E-04
14	0	1	0	3.39E-04	1.30E-04	4.56E-04	1.30E-04
15	0	1	0	1.24E-03	2.65E-04	1.06E-03	2.65E-04
16	0.29	0.40	0.31	8.52E-04	3.07E-04	4.65E-04	1.36E-04
17	0	1	0	1.36E-03	3.92E-04	1.06E-03	3.92E-04
18	0.28	0.42	0.30	3.81E-04	6.65E-05	2.17E-04	8.68E-05
19	0.33	0.43	0.25	1.30E-03	1.45E-03	2.28E-03	5.02E-04
20	0.00	0.55	0.45	9.65E-04	2.38E-04	1.32E-03	2.55E-04

recommendations in sea wave research. The headings were independent and randomly selected, denoted by ψ_n .

Their RIC distributions were pre-calculated as illustrated in Fig. 5(a), and then applied as the basis of multispectral fusion procedure. A threshold value $\eta = 0.15$ was employed. Consequently, if the weight dropped below η , the corresponding estimate was deemed unreliable.

B. Results

Although, the effectiveness of the WBA performance assessment criterion was preliminarily discussed in Section III, additional observations related to Fig. 5 could be made. Despite the similar patterns observed in the local RIC distribution and the WBA performance, the geometry and size of the ships are additional factors that influence sea state estimation. Ship 3, the largest ship, displayed the most pronounced low-pass characteristics. The low-value portion of the local RIC was situated in the lower frequency region, indicating that the larger vessel exhibited superior performance when

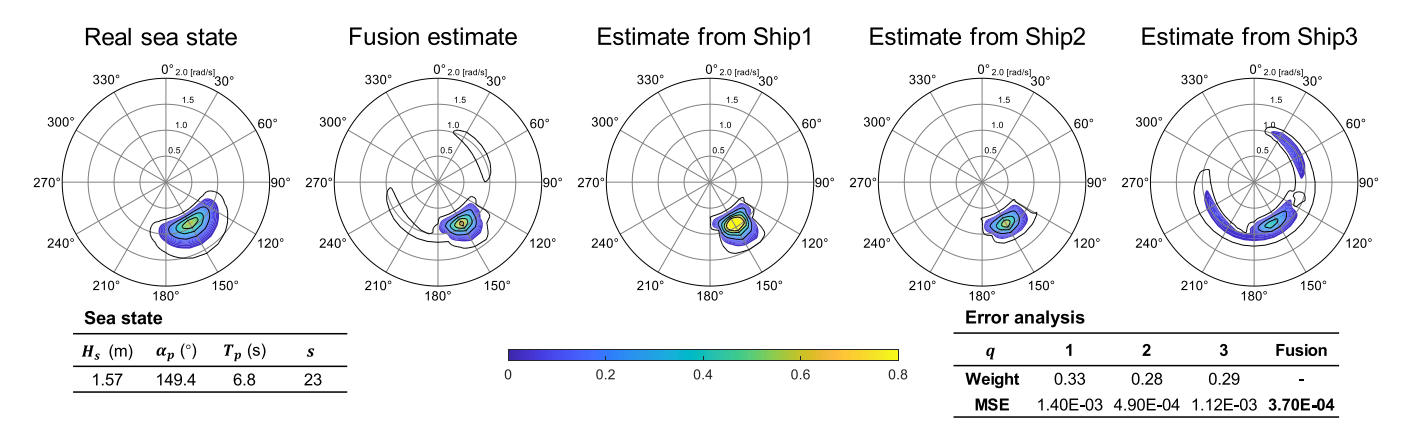


Fig. 8. Estimates obtained from the WBA of multiple ships and the fusion estimate, as compared to the real sea state (Sea state 1).

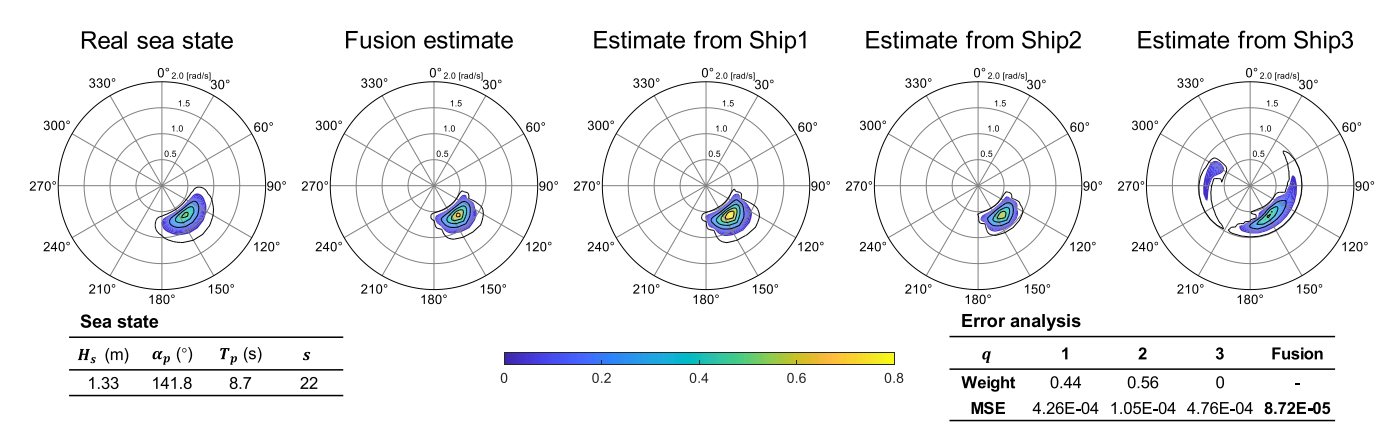


Fig. 9. Estimates obtained from the WBA of multiple ships and the fusion estimate, as compared to the real sea state (Sea state 2).

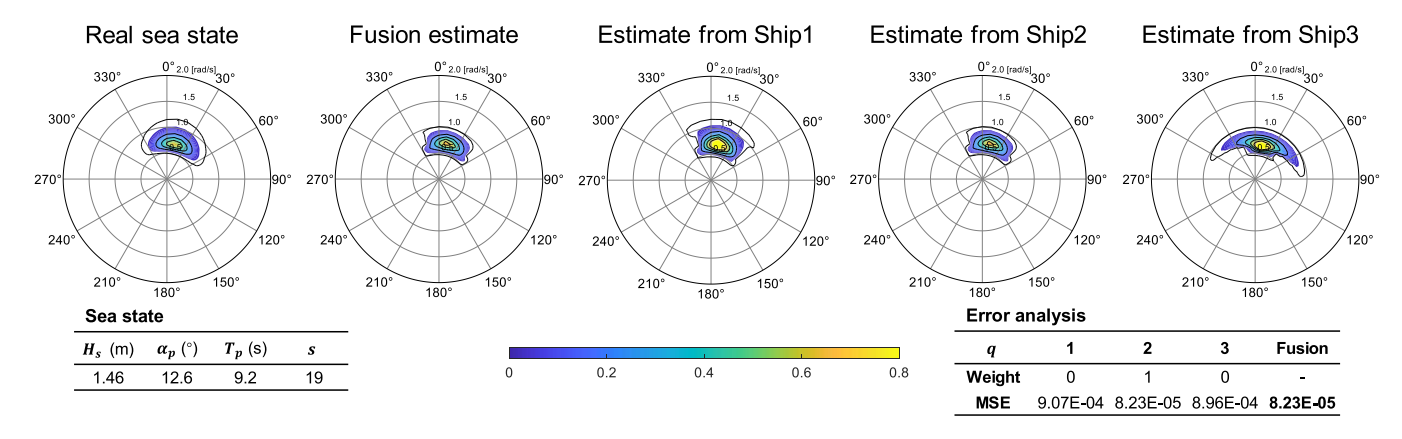


Fig. 10. Estimates obtained from the WBA of multiple ships and the fusion estimate, as compared to the real sea state (Sea state 3).

encountering low-frequency sea states, which was confirmed in simulations. Conversely, the smallest ship, Ship 1, exhibited much better performance in relatively high-frequency waves. Generally, smaller ships demonstrated a more comprehensive capacity to handle different wave conditions.

Simulations were conducted under all the listed sea states and several typical cases, illustrated in Fig. 8-11, are included here to demonstrate the significant effectiveness of the multispectral fusion. The colorbar in the figure represents the energy distribution, with the blue indicating zero energy and yellow representing the upper limit. In Fig. 8, estimates obtained from multiple ships failed to accurately replicate

the real-time wave spectrum. The directional wave spectrum from Ship1 feature a higher and more concentrated energy distribution. In contrast, the estimates from the other two ships displayed lower energy levels as compared to the real sea state. By employing different weights to multiple estimates, the estimation error of the fusion spectrum derived from the multispectral fusion algorithm significantly decreased. In Sea State 2, the estimate from Ship 3 was regarded as unreliable in the fusion process. The simulation results supported this decision, as the wave spectrum from Ship 3 became diffused and recorded the highest MSE. Conversely, the estimates from the first two ships were closer to the real situation. The fusion

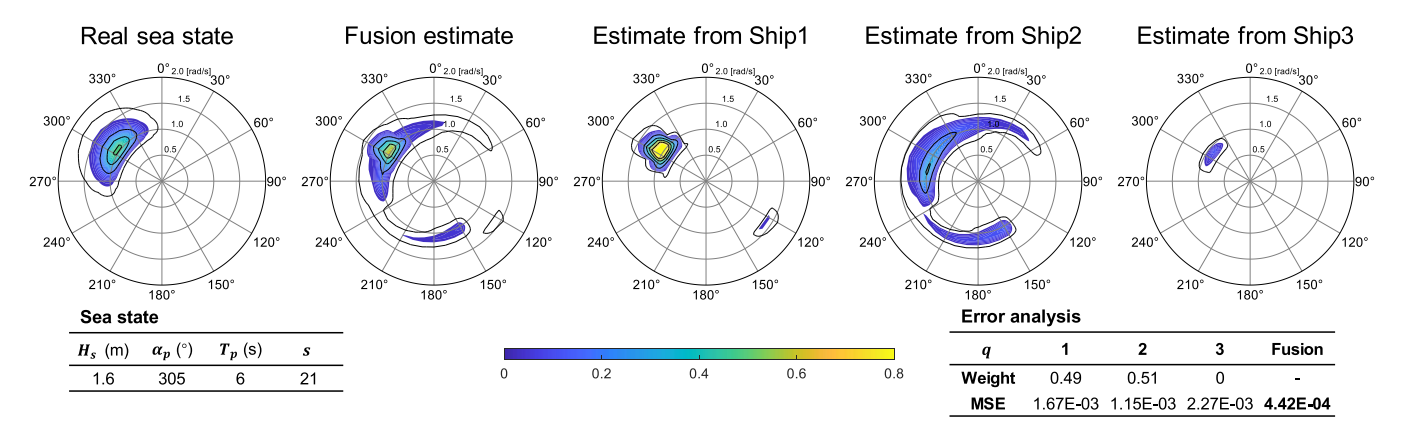


Fig. 11. Estimates obtained from the WBA of multiple ships and the fusion estimate, as compared to the real sea state (Sea state 4).

result derived from these two estimates demonstrated further reduced error, as shown in Fig. 9.

Simulation under Sea state 3 displayed a special case because all three weighted parameters from the assessment criteria fell below the threshold value. Hence, the fusion algorithm regarded the most reliable estimate as the final result. The simulation result showed that the selected estimate was the most accurate. Hence, it is possible to exclude the distraction from unreliable estimates to obtain an accurate result with the support of the RIP-based assessment (see Fig. 10). In Sea state 4, the waves exhibited high-frequency characteristics (see Fig. 11). The largest ship, Ship 3, completely failed to estimate the sea state and had no contribution in the fusion process. Under such high-frequency conditions, the estimates from the other two ships were also suboptimal. However, with the involvement of the proposed fusion method, the final estimate derived from the fusion algorithm substantially reduced the estimation error.

The weight distribution and error analysis results for other sea states are tabulated in TABLE III. The minimum error values for multiple estimates and fused results are indicated in bold. It was evident that the fusion algorithm significantly enhanced the accuracy of the sea state estimations in most cases. Even in situations where all three estimates were deemed unreliable, the algorithm successfully identified the most accurate spectrum as the final estimate. In the few cases where the fused result did not improve the error compared to the best estimates from the three ships. The errors were roughly equivalent to those of the most accurate ship. Hence, the results were generally considered to have no negative impact on the accuracy of the existing estimates.

VI. CONCLUSION

Using oscillating ships as wave buoys supplements existing methods, providing an alternative option to derive real-time on-site wave information by utilizing only motion sensors. However, the WBA concept is built on many ideal assumptions and is constrained by the ship's inherent hydrodynamic properties. This study aims to interpret the relationship between the transfer functions constructed by RAOs and wave estimate accuracy from the perspective of RIP. The proposed RIP-based assessment criterion can be used to evaluate the

reliability of estimates from the WBA. It is valuable for determining whether a ship can achieve an effective estimate and for avoiding erroneous estimates that could mislead onsite decision-making. Considering that marine operations often involve different types of ships and lack sufficient sea state information, a RIP-based multispectral fusion algorithm was proposed to combine the estimates obtained from multiple ships, using local RIC values as the weighting basis. Simulations were conducted with three ships of different sizes, proving the effectiveness of the proposed criterion and fusion approach.

The current study aims to explain the inherent problems faced by WBA in theoretical terms. Multispectral fusion is presented as a possible application scenario since ships have different estimation performances when facing incoming waves. Model tests and sea trials are needed to further demonstrate the applicability and effectiveness of the proposed methods. There are some issues that need to be discussed. In water tank tests, producing short-crest irregular waves is extremely difficult, and addressing the scale effect is a challenge. In sea trials, setting a benchmark is problematic. Existing works often use large-scale observations like satellites, which have poor resolution and considerable delay. The best solution is to directly collect data from ships equipped with wave radar and motion monitoring systems for crossing contrast.

From the perspective of the WBA area, there are some limitations that need to be addressed. The assumption of a perfect RAO is too ideal, as a ship's hydrodynamics vary with different draughts and changes in working status. The hybrid approach, combining an online training data-driven model and a model-based method, is a considerable prospect. The assumption of a stationary sea state is another limitation. While it is acceptable for long-term service, in the scenario of WBA applications where real-time wave spectrum calculations are required, the time-varying properties of the sea state should be considered in future research.

REFERENCES

[1] Y. Li, N. Ren, W. Cai, Y. Liu, and J. Ou, "Experimental and numerical study on dynamic responses of a TLP-type modular floating structure system," *Ocean Eng.*, vol. 313, Dec. 2024, Art. no. 119427.

- [2] Z. Ren, R. Skjetne, A. S. Verma, Z. Jiang, Z. Gao, and K. H. Halse, "Active heave compensation of floating wind turbine installation using a catamaran construction vessel," *Mar. Struct.*, vol. 75, Jan. 2021, Art. no. 102868.
- [3] A. Y. Elghazouli, A. Mujdeci, D. V. Bompa, and Y. T. Guo, "Experimental cyclic response of rubberised concrete-filled steel tubes," J. Constructional Steel Res., vol. 199, Dec. 2022, Art. no. 107622.
- [4] Y. Shu et al., "Reference path for ships in ports and waterways based on optimal control," *Ocean Coastal Manage.*, vol. 253, Jul. 2024, Art. no. 107168.
- [5] M. Burhan, Q. Chen, M. W. Shahzad, D. Ybyraiymkul, F. H. Akhtar, and K. C. Ng, "Innovative concentrated photovoltaic thermal (CPV/T) system with combined hydrogen and MgO based storage," *Int. J. Hydrogen Energy*, vol. 46, no. 31, pp. 16534–16545, May 2021.
- [6] S. Wang and T. Moan, "Methodology of load effect analysis and ultimate limit state design of semi-submersible hulls of floating wind turbines: With a focus on floater column design," Mar. Struct., vol. 93, Jan. 2024, Art. no. 103526.
- [7] F. Ardhuin et al., "Observing sea states," Frontiers Mar. Sci., vol. 6, p. 124, Apr. 2019.
- [8] W. Huang, X. Liu, and E. Gill, "Ocean wind and wave measurements using X-band marine radar: A comprehensive review," *Remote Sens.*, vol. 9, no. 12, p. 1261, Dec. 2017.
- [9] D. C. Stredulinsky and E. M. Thornhill, "Ship motion and wave radar data fusion for shipboard wave measurement," *J. Ship Res.*, vol. 55, no. 2, pp. 73–85, Jun. 2011.
- [10] A. C. Brown and R. K. Paasch, "The accelerations of a wave measurement buoy impacted by breaking waves in the surf zone," *J. Mar. Sci. Eng.*, vol. 9, no. 2, p. 214, Feb. 2021.
- [11] K. Lindemann, J. Odland, and J. Strengtheagen, "On the application of hull surveillance systems for increased safety and improved structural utilization in rough weather," Soc. Naval Architects Marine Eng., Jersey City, NJ, USA, Tech. Rep., 1977.
- [12] J. N. Newman, Marine Hydrodynamics. Cambridge, MA, USA: MIT Press, 2018.
- [13] U. D. Nielsen, "Estimation of directional wave spectra from measured ship responses," in *Maritime Transportation and Exploitation of Ocean and Coastal Resources*, C. Guedes Soares, Y. Garbatov, and N. Fonseca, Eds., New York, NY, USA: Taylor & Francis, Aug. 2006, pp. 1103–1112.
- [14] U. D. Nielsen and J. Dietz, "Ocean wave spectrum estimation using measured vessel motions from an in-service container ship," *Mar. Struct.*, vol. 69, Jan. 2020, Art. no. 102682.
- [15] K. Hasselmann et al., "Measurements of wind-wave growth and swell decay during the joint north sea wave project (JONSWAP)," *Ergänzung-sheft 8-12*, vol. 12, p. 95, Jan. 1973.
- [16] P. Han, G. Li, X. Cheng, S. Skjong, and H. Zhang, "An uncertainty-aware hybrid approach for sea state estimation using ship motion responses," *IEEE Trans. Ind. Informat.*, vol. 18, no. 2, pp. 891–900, Feb. 2022.
- [17] R. Pascoal and C. Guedes Soares, "Non-parametric wave spectral estimation using vessel motions," *Appl. Ocean Res.*, vol. 30, no. 1, pp. 46–53, Feb. 2008.
- [18] U. D. Nielsen, "Estimations of on-site directional wave spectra from measured ship responses," *Mar. Struct.*, vol. 19, no. 1, pp. 33–69, Jan. 2006.
- [19] J. Wang, Y. Ren, W. Shi, M. Collu, V. Venugopal, and X. Li, "Multi-objective optimization design for a 15 MW semisubmersible floating offshore wind turbine using evolutionary algorithm," *Appl. Energy*, vol. 377, Jan. 2025, Art. no. 124533.
- [20] Z. Ren, X. Han, A. S. Verma, J. A. Dirdal, and R. Skjetne, "Sea state estimation based on vessel motion responses: Improved smoothness and robustness using Bézier surface and L1 optimization," *Mar. Struct.*, vol. 76, Mar. 2021, Art. no. 102904.
- [21] T. Iseki and K. Ohtsu, "Bayesian estimation of directional wave spectra based on ship motions," *Control Eng. Pract.*, vol. 8, no. 2, pp. 215–219, 2000.
- [22] U. D. Nielsen, "Introducing two hyperparameters in Bayesian estimation of wave spectra," *Probabilistic Eng. Mech.*, vol. 23, no. 1, pp. 84–94, Ian. 2008
- [23] R. Pascoal, L. P. Perera, and C. G. Soares, "Estimation of directional sea spectra from ship motions in sea trials," *Ocean Eng.*, vol. 132, pp. 126–137, Mar. 2017.
- [24] F. Tu, S. S. Ge, Y. S. Choo, and C. C. Hang, "Sea state identification based on vessel motion response learning via multi-layer classifiers," *Ocean Eng.*, vol. 147, pp. 318–332, Jan. 2018.

- [25] M. Liu, X. Cheng, F. Shi, X. Liu, H. Dai, and S. Chen, "A prototype-empowered kernel-varying convolutional model for imbalanced sea state estimation in IoT-enabled autonomous ship," *IEEE Trans. Sustain. Comput.*, vol. 9, no. 6, pp. 862–873, Nov. 2024.
- [26] T. Kawai, Y. Kawamura, T. Okada, T. Mitsuyuki, and X. Chen, "Sea state estimation using monitoring data by convolutional neural network (CNN)," J. Mar. Sci. Technol., vol. 26, no. 3, pp. 947–962, Sep. 2021.
- [27] P. Han, G. Li, S. Skjong, and H. Zhang, "Directional wave spectrum estimation with ship motion responses using adversarial networks," *Mar. Struct.*, vol. 83, May 2022, Art. no. 103159.
- [28] S. Li et al., "A novel robustness-enhancing adversarial defense approach to AI-powered sea state estimation for autonomous marine vessels," *IEEE Trans. Syst., Man, Cybern., Syst.*, vol. 55, no. 1, pp. 28–42, Jan. 2025.
- [29] L. Zhou, Q. Sun, S. Ding, S. Han, and A. Wang, "A machine-learning-based method for ship propulsion power prediction in ice," *J. Mar. Sci. Eng.*, vol. 11, no. 7, p. 1381, Jul. 2023.
- [30] U. D. Nielsen, A. H. Brodtkorb, and A. J. Sørensen, "Sea state estimation using multiple ships simultaneously as sailing wave buoys," *Appl. Ocean Res.*, vol. 83, pp. 65–76, Feb. 2019.
- [31] M. Vidyasagar, An Introduction to Compressed Sensing. Philadelphia, PA, USA: SIAM, 2019.
- [32] D. L. Donoho, "Compressed sensing," *IEEE Trans. Inf. Theory*, vol. 52, no. 4, pp. 1289–1306, Apr. 2006.
- [33] E. J. Candes and T. Tao, "Decoding by linear programming," *IEEE Trans. Inf. Theory*, vol. 51, no. 12, pp. 4203–4215, Dec. 2005.
- [34] R. Baraniuk, "Compressive sensing [lecture notes]," *IEEE Signal Process. Mag.*, vol. 24, no. 4, pp. 118–121, Jul. 2007.
- [35] R. Skjetne and Z. Ren, "A survey on modeling and control of thrusterassisted position mooring systems," *Mar. Struct.*, vol. 74, Nov. 2020, Art. no. 102830.
- [36] U. D. Nielsen, "Estimation of directional wave spectra from measured ship responses," in *Proc. 12th Int. Congr. Int. Maritime Assoc. Medit.*, 2005, pp. 1103–1112.
- [37] A. Bakushinsky and A. Goncharsky, *Ill-Posed Problems: Theory and Applications*, vol. 301. Cham, Switzerland: Springer, 2012.
- [38] W. Dai and O. Milenkovic, "Subspace pursuit for compressive sensing signal reconstruction," *IEEE Trans. Inf. Theory.*, vol. 55, no. 5, pp. 2230–2249, May 2009.



Taiyu Zhang received the B.Eng. degree in hydraulic engineering from Tianjin University, Tianjin, China, in 2022. He is currently pursuing the Ph.D. degree with the Institute for Ocean Engineering, Tsinghua University, Shenzhen, China. His current research interests include spectral analysis, wave perception, and time-varying systems.



Zhengru Ren received the B.Eng. degree in ocean engineering from Dalian University of Technology, Dalian, China, in 2012, and the M.Sc. and Ph.D. degrees in marine technology from the Norwegian University of Science and Technology (NTNU), Trondheim, Norway, in 2015 and 2019, respectively. From 2019 to 2021, he was a Post-Doctoral Research Fellow with the Centre for Research-Based Innovation on Marine Operations (SFI MOVE), Department of Marine Technology, NTNU. He is currently an Assistant Professor with the Institute for Ocean

Engineering, Tsinghua University, Shenzhen, China. His research interests include nonlinear control theory, sensor fusion, intelligent and digitalized ocean engineering, and offshore wind energy.